J Appl Electrochem (2012) 42:843–850
DOI 10.1007/s10800-012-0449-6

ORIGINAL PAPER

Effects of the phase constitution and microstructure on the electrochemical properties of melt-spun $Al_{88-X}Si_{12}Mn_X$ anode materials for lithium-ion batteries

Zhang Linping · Lu Feifei · Song Xianlei · Liang Pu · Wang Fei · Sun Zhanbo · Li Xuepeng · Song Xiaoping

Received: 5 April 2012 / Accepted: 3 July 2012 / Published online: 15 July 2012

Abstract The phase constitution, microstructure, electrochemical properties, and lithiation mechanism of the melt-spun $Al_{88-X}Si_{12}Mn_X$ ($X = 1$, 3, 5, 7, 10, 13, 15, mol%) ribbons were investigated as anode materials for lithium-ion batteries. When $X = 1$ and 3, the alloys were composed of coarse supersaturated α-Al grains and fine α-Si grains spread along the boundaries, and performed high initial capacities but fast capacity fade. As X was increased to 5 and 7, the constitution of alloys was characterized by nanoscaled α-Al and amorphous regions, and they exhibited capacities of 924 and 764 mAh g^{-1} initially, 733 and 578 mAh g^{-1} at the second cycle and then maintained 391 and 351 mAh g^{-1} after 50 cycles, respectively. When the Mn content was more than 10 %, an intermetallic compound $Al_{4.01}MnSi_{0.74}$ co-existed with α-Al and it evolved into the predominated constitution. The initial specific capacities were very high, but faded rapidly only experiencing few cycles. After lithiation, any compound with Li could not be detected in the $Al_{85}Si_{12}Mn_3$ and $Al_{83}Si_{12}Mn_5$ anodes, while the AlLi intermetallic compound could be detected when the Mn content was increased to 13 %. It could be considered that the appropriate phase constitution and microstructure in the $Al_{83}Si_{12}Mn_5$ and $Al_{81}Si_{12}Mn_7$ anodes were very beneficial to mitigating structure evolution, improving structure stability, and obtaining favorable electrochemical properties. The $Al_{4.01}MnSi_{0.74}$ compound was an active phase for Li storage in the present system, but it was responsible for serious structure evolution, poor cyclability, and pulverization.

Keywords Al–Si–Mn alloy · Melt spinning · Lithium-ion batteries · Phase constitution · Microstructure · Electrochemical properties

1 Introduction

In order to meet the ever-increasing demand for lithium-ion batteries with higher energy density, alternative anode materials of conventional graphite have been extensively investigated. Some alloys (Sn, Sb, Al, etc.) are considered as the most promising materials to be used in advanced design because of their high capacities. Recently, materials such as metal-based alloys, nanomaterials, composite materials, and porous materials have been the focus of research on improving the cyclability [1–5].

However, the critical problem that limits the commercial application of alloy anodes is the severe structure evolution during lithiation/delithiation, which leads to inevitable pulverization of materials and rapid capacity fade. Accordingly, many great efforts have been devoted to overcome the problem, e.g., exploiting composite materials which are constituted of electrochemically active materials embedded in an inactive matrix. Meanwhile, various synthesis methods, such as ball milling, reductive precipitation, magnetron sputtering, and melt spinning [6–9], have been adopted to obtain special structures to further improve the cycle performance. Several materials, such as Al, Sn, Sb, Si, etc. [10–13], exhibit improved cycling performance owing to the buffering effect of inactive components in the alloys that can enhance the structural stability during cycling. Though excellent electrochemical properties with

Z. Linping · L. Feifei · S. Xianlei · L. Pu · W. Fei · S. Zhanbo (✉) · L. Xuepeng · S. Xiaoping
MOE Key Laboratory for Non-equilibrium Synthesis and Modulation of Condensed Matter, State Key Laboratory for Mechanical Behavior of Materials, Xi'an Jiaotong University, Xi'an 710049, China
e-mail: szb@mail.xjtu.edu.cn

high capacity and favorable cycle performance have been obtained in nanomaterials, they are difficult to be produced in a large scale, which significantly limits their application to high-energy lithium-ion batteries.

According to Hauser's literatures [14], the Al–Si–Mn alloy system with a special composition range could be prepared into metallic glass, so the addition of the third component Mn could improve the solubility of Si in α-Al in the melt-spun alloys and form supersaturated solid solution α-Al. In our previous work [15, 16], ternary $Al_{60-X}Si_{40}Mn_X$ and $Al_{70-X}Si_{30}Mn_X$ alloys were prepared by melt spinning as anode materials for lithium-ion batteries. The cyclability could be improved obviously by the addition of the inert component which could alleviate the volume variation during charge/discharge processes. Under the condition of melt spinning, thermodynamical non-equilibrium $Al_{60-X}Si_{40}Mn_X$ [15] and $Al_{70-X}Si_{30}Mn_X$ [16] alloys with a special state and structure could restrain the structure evolution and improve the cycle performance than equilibrium alloys. The alloys with a certain composition exhibited favorable cyclability as well as high specific capacities. The α-Al, α-Si and Al/Si/Mn compounds co-existed in the alloys when the Mn content was higher than 7 % and the volume fraction of Al/Si/Mn compounds increased as the Mn content augmented. When the Mn content was increased to 10 %, plenty of Al/Si/Mn compounds formed in the alloys and the capacity became much lower. Therefore, it could be speculated that the Al/Si/Mn compounds in the systems did not react with Li. Besides, the work indicated that neither α-Si was alloyed with Li nor did the Al–Li intermetallic compounds form during lithiation caused by the inhibitory action of multiphase. Although obvious pulverization did not appear in the anodes, the serious cracks and shedding, which were responsible for capacity fade, were observed. However, the existence of superabundant coarsening Al/Si/Mn compounds and α-Si which would decrease the toughness and plasticity had a negative effect on the cyclability. Thus, we considered to reduce the Si content to improve the cycle performance by decreasing the fraction of the superabundant Al/Si/Mn compounds and α-Si in the as-quenched ribbons.

In this article, the electrochemical performance and reaction mechanism of melt-spun Al–Si–Mn alloys with the low Si content (12 %) and Mn content in a wide range of 1–15 % were investigated. The influence of law of phase constitution and microstructure on the electrochemical properties and lithiation mechanism was analyzed. When the Mn content was in a range of 5–7 %, the alloys exhibited favorable electrochemical properties because they were mainly composed of single supersaturation solid solution of α-Al in the nanoscaled and amorphous regions which had excellent mechanical properties. As the Mn content was increased over 10 %, the $Al_{4.01}MnSi_{0.74}$ compound formed as an active phase for Li storage in the present system, resulting in serious structure evolution, pulverization, and poor cyclability.

2 Experimental

Pure aluminum (99.95 wt%), pure silicon (99.99 wt%), and pure manganese (99.95 wt%) were used to prepare the Al–Si–Mn alloys. The raw materials were arc melted employing a non-consumable tungsten electrode under the protection of Ar. The alloy ingots were put into quartz tubes with the bottom holes of Φ1 mm in diameter, heated by high-frequency induction, fully melted, and then blown from the bottom holes to a cooling roller of Φ250 mm in diameter to quench into ribbons with a velocity of 2,500 rpm. The obtained ribbons were about 3 mm in width and 30 μm in thickness. Their phase constitutions were analyzed using a Bruker D8 advanced X-ray diffractometer (XRD) with the Cu Kα radiation at an operating voltage of 40 kV and operating current of 40 mA, and the thermodynamic states were tested by a NETZSCH STA-449C Simultaneous Thermal Analyzer in a temperature range from 323 to 800 K and at a heating rate of 10 K min^{-1}. The microstructures were observed by a JEM-2100 transmission electron microscope (TEM), and the foil specimens used for TEM were prepared by ion polishing. The phase constitutions and microstructure analysis of the ball-milled powder and the specimen after heating were carried out.

The as-quenched ribbons were prepared into powders by ball milling for 1 h under Ar gas protection, and then mixed homogeneously with carbon black. The mixture was blended with polyvinylidene fluoride (PVDF) dissolved in *N*-methylpyrrolidinone (NMP). The mass ratio of the powders, carbon black, and PVDF was 84:8:8. The slurry was evenly coated on a copper foil and dried at 373 K in a vacuum oven for 10 h to remove the NMP. Simulation cells were assembled in a dry glove box filled with pure Ar. The electrochemical measurements were carried out in the two-electrode Swagelok cells which were composed of alloy anode as the working electrode, a pure lithium foil as the counter electrode, Celegard 2400 as the separator, and 1 M LiPF6 in ethylene carbonate (EC)–diethyl carbonate (DEC) (1:1, v/v) as the electrolyte. The electrochemical performance of electrodes was measured by an Arbin BT-2000 Instrument under a constant current density of 0.05 A g^{-1}. The low cutoff voltages were set to 0.03 V, while the high cutoff was 1.0 V in the cycles. The cyclic voltammetric measurements were measured by a VersaSTAT MC instrument at a scanning speed of 0.1 mV/s between 0 and 1.5 V. The structures of the lithiated anodes were analyzed by the XRD, and the surface morphology of

the anodes after cycles was observed using a JSM-7000F Scanning Electron Microscope (SEM).

3 Results

The XRD patterns of the melt-spun $Al_{88-X}Si_{12}Mn_X$ ($X = 1$, 3, 5, 7, 10, 13, and 15 mol%) ribbons and ball-milled $Al_{83}Si_{12}Mn_5$ samples are shown in Fig. 1. In the patterns, the diffraction peaks of α-Al and α-Si when $X = 1$ and 3, but only the peaks of α-Al appeared as $X = 5$ or 7. Such results indicated that the α-Si phase disappeared when the alloys contained 5 and 7 % Mn, which was different from the melt-spun Al–Si–Mn alloys with 30 % [16] and 40 % Si [15], where diffraction peaks of α-Si were always detected. Besides, the peaks of the intermetallic compound $Al_{4.01}MnSi_{0.74}$, as denoted by "▼," were observed in $Al_{88-X}Si_{12}Mn_X$ when $X = 10$, 13, and 15. The compound contained a high content of Al and was different from that in the melt-spun Al–Si–Mn with 30 and 40 % Si [15, 16]. When the Mn content was in a range of 1–7 %, the length of obtained ribbons were unlimited and they showed better plasticity and toughness, compared with those of Al–Si–Mn alloys with high Si content [15, 16]. Moreover, additional diffraction peaks could not be observed in the XRD patterns of the ball-milled $Al_{83}Si_{12}Mn_5$ samples, which indicated that the phase composition did not change after ball milling.

Figure 2 shows the microstructures of the as-quenched $Al_{88-X}Si_{12}Mn_X$ ($X = 1$, 5, 7, and 13) ribbons and ball-milled $Al_{83}Si_{12}Mn_5$ samples. For the $Al_{87}Si_{12}Mn_1$ ribbons, the size of the α-Al grains was more than 200 nm and some nano-scaled α-Si particles that were much finer than those in the previous studies [15, 16] spread along the grain boundaries, as seen in Fig. 2a. It should be noticed that the amorphous regions, as denoted by the white arrows in Fig. 2b, c, distributed among the nano-scaled α-Al grains in the as-quenched $Al_{83}Si_{12}Mn_5$ and $Al_{81}Si_{12}Mn_7$ ribbons. The existence of the amorphous regions resulted in the decrease of the α-Al peak intensity in the XRD patterns (Fig. 1). Moreover, the α-Al grains in the as-quenched $Al_{81}Si_{12}Mn_7$ were smaller than those in the $Al_{83}Si_{12}Mn_5$ ribbons. However, for $Al_{75}Si_{12}Mn_{13}$, the amorphous regions disappeared, and the coarse intermetallic compound and α-Al grains spread alternatively, as shown in Fig. 2d. After ball milling, the amorphous regions still existed, and the variation of the microstructure could not be observed (Fig. 6e). It can be concluded that the content of Mn has a considerable influence on the microstructure, and that the appearance of the intermetallic compound evidently leads to an obvious reduction of plasticity and toughness. The results show that the ball-milling process has no obvious influence on the phase composition or the microstructure.

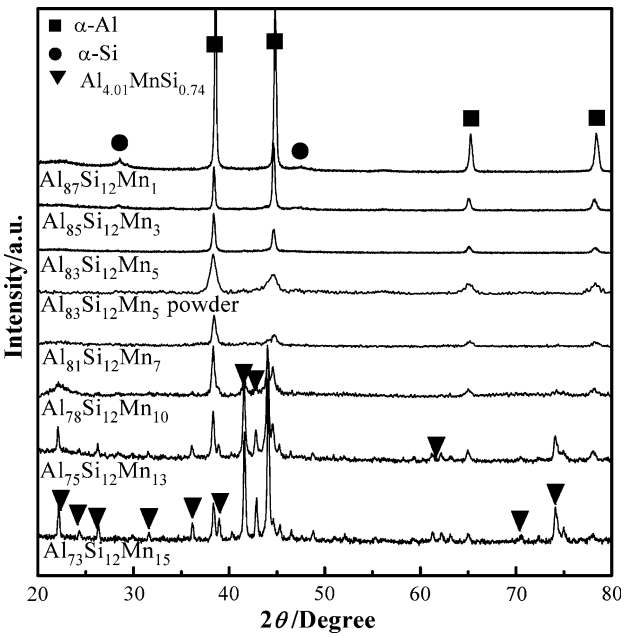

Fig. 1 XRD diffraction patterns of melt-spun $Al_{88-X}Si_{12}Mn_X$ ribbons and ball-milled $Al_{83}Si_{12}Mn_5$ samples

Figure 3 presents the Differential Scanning Calorimetry (DSC) curves of the melt-spun $Al_{88-X}Si_{12}Mn_X$ ($X = 3$, 5, 7, 10, and 13) ribbons and the XRD patterns of the specimen after heating. The distinct exothermal peaks during 550–700 K appeared in the DSC curves, indicating that the alloys were in a non-equilibrium state, as shown in Fig. 3a. After the heating process, the diffraction peaks of α-Al, α-Si, and $Al_{4.01}MnSi_{0.74}$ became much stronger, as seen in Fig. 3b. So, the exothermal peaks indicated the crystallization of amorphous regions ($X = 5$, 7), the decomposing of the supersaturated solid solution, and the formation of intermetallic compounds.

Figure 4 illustrates that the discharge-specific capacity of the melt-spun $Al_{88-X}Si_{12}Mn_X$ alloys depends on cycle numbers. The $Al_{87}Si_{12}Mn_1$ had the higher discharge capacity of 1,243 mAh g^{-1} at the first cycle; it stayed stable in the following few cycles and then gradually faded to 238 mAh g^{-1} during the rest 25 cycles. The $Al_{85}Si_{12}Mn_3$ also presented the similar capacity tendency. When the Mn content was increased to 5 and 7 %, the anodes exhibited capacities of 924 and 764 mAh g^{-1} initially, 733 and 578 mAh g^{-1} the second cycle, and maintained reversible capacities of 391 and 351 mAh g^{-1} after 50 cycles, respectively. The cyclability was improved compared with our previous work [15, 16]. However, when the Mn content was increased to 10 %, the discharge-specific capacity of 855 mAh g^{-1} could be obtained in the 1st cycle, and the retention was 50 % in the next one. Its capacity could be kept stable during the following 15 cycles and then declined quickly. As the Mn content was 13 %, the discharge-specific

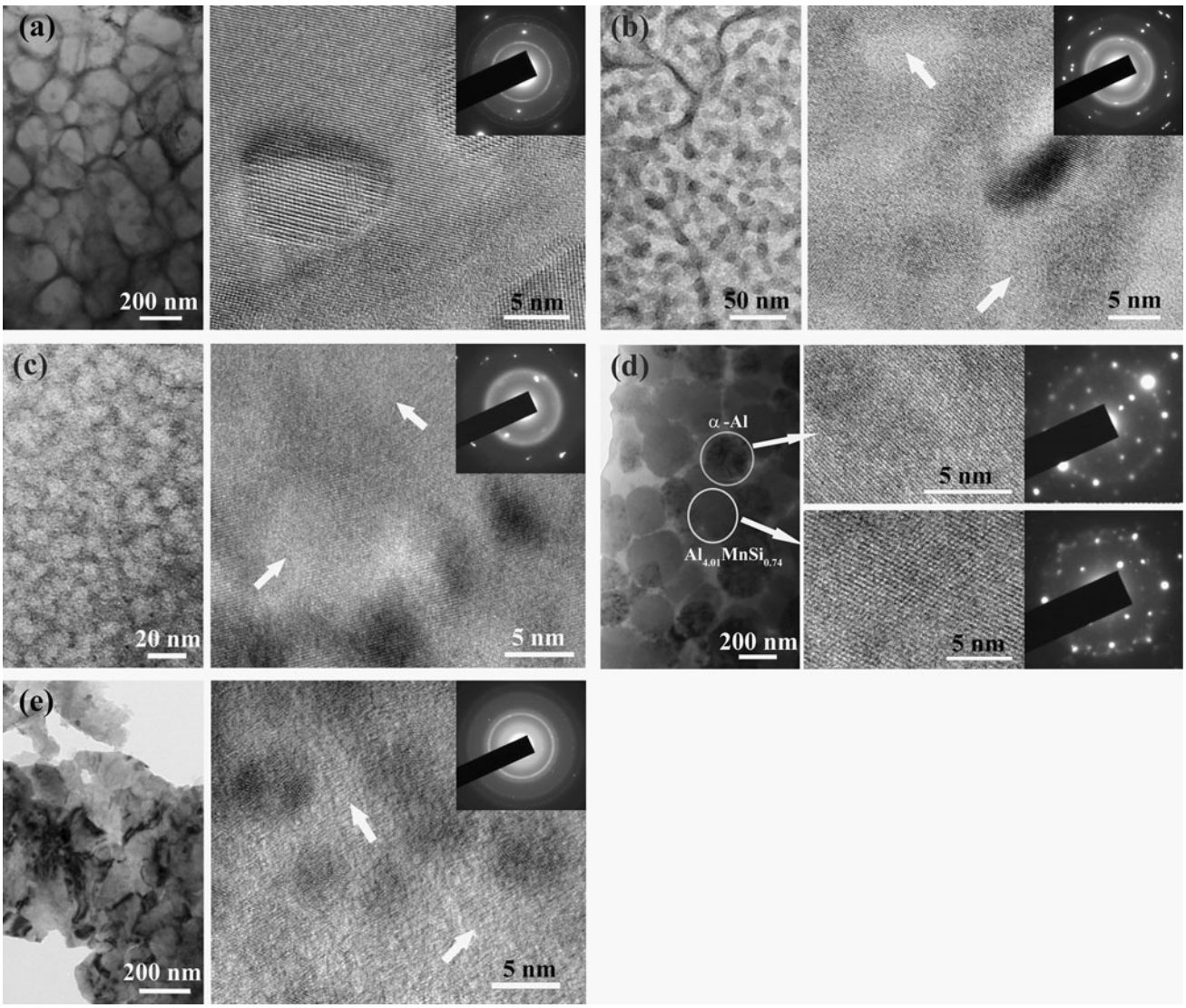

Fig. 2 Microstructures of the as-quenched $Al_{87}Si_{12}Mn_1$ (**a**), $Al_{83}Si_{12}Mn_5$ (**b**), $Al_{81}Si_{12}Mn_7$ (**c**) and $Al_{75}Si_{12}Mn_{13}$ (**d**) ribbons and ball-milled $Al_{83}Si_{12}Mn_5$ samples (**e**). The *arrows* denote the amorphous regions

capacity could reach to a value of 1,176 mAh g^{-1} in the first cycle, and faded quickly to 33 mAh g^{-1} over 4 cycles. A highest discharge capacity of 1,521 mAh g^{-1} was exhibited in the first cycle, but it decreased drastically to 27 mAh g^{-1} in the next cycle for $Al_{73}Si_{12}Mn_{15}$.

The X-ray diffraction patterns of the lithiated anodes are shown in Fig. 5. For the patterns of the anodes prepared from the as-quenched $Al_{85}Si_{12}Mn_3$ and $Al_{83}Si_{12}Mn_5$ ribbons, any diffraction peaks of compounds with Li could not be clearly measured. When the Mn content was increased to 13 %, the diffraction peaks of the AlLi intermetallic compound were detected although the diffraction characteristics of the peaks were close to some of $Al_{4.01}MnSi_{0.74}$. Because of the high initial capacity shown in the melt-spun $Al_{88-X}Si_{12}Mn_X$ when $X = 10$, 13, and 15, it could be concluded that the Al/Si/Mn compound in this work was alloyed by Li. The result was not present in our prior work.

Figure 6 displays the cyclic voltammetric curves for the as-quenched $Al_{88-X}Si_{12}Mn_X$ ($X = 1$, 5, 7, and 13) anodes. In general, the current peaks respond to lithiation/delithiation reaction, and every anode material has distinctive current peaks. The cathodic current peak which appeared at about 0.6 V in the first cycle was due to the formation of the solid electrolyte interphase (SEI) according to the published work [17], which may lead to the initial irreversible capacity. According to Lee point [18], Li occurred in the alloying reaction with anodes at a specific voltage, which led to sharp current peaks, but they would disappear if Li dissolved in the anodes and formed solid solution at a wider range of voltage. As shown in Fig. 6a, the anodic

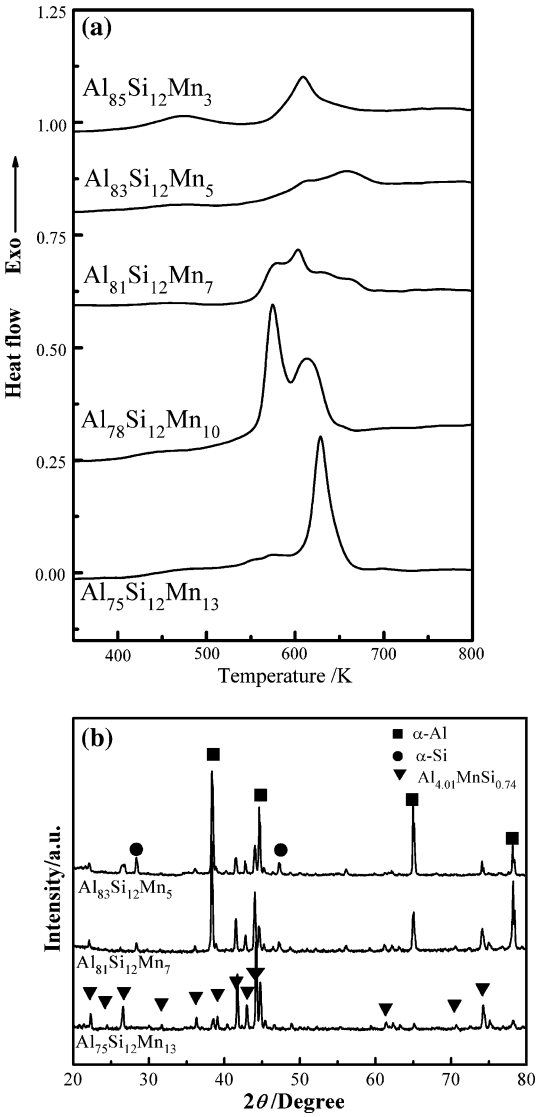

Fig. 3 Differential scanning calorimetry curves of the as-quenched $Al_{88-X}Si_{12}Mn_X$ ($X = 3, 5, 7, 10, 13$) ribbons and XRD diffraction patterns of the specimens after heating

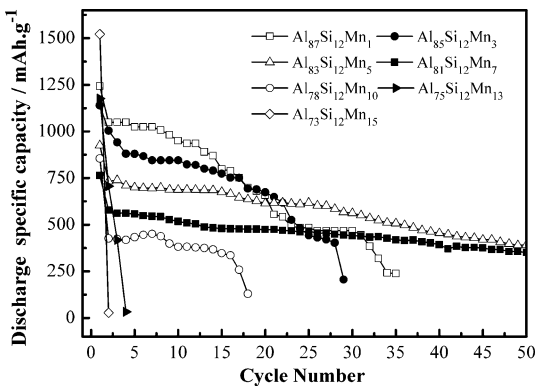

Fig. 4 Cycle performance of the as-quenched $Al_{88-X}Si_{12}Mn_X$ ($X = 1, 3, 5, 7, 10, 13$, and 15) alloy anodes

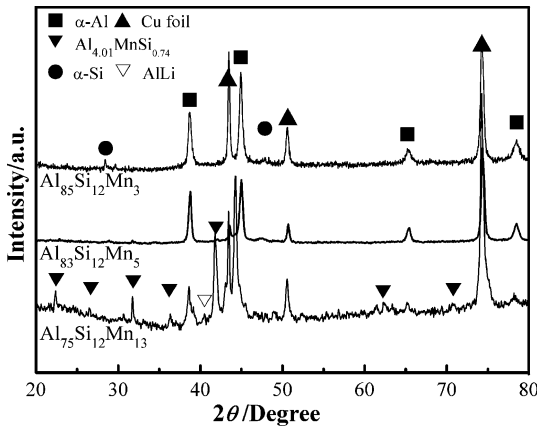

Fig. 5 X-ray diffraction patterns of the lithiated anodes prepared from the as-quenched $Al_{88-X}Si_{12}Mn_X$ ($X = 3, 5, 13$) alloy anodes

current peaks around 0.65 V resulted from the delithiation reaction. However, the cathodic peak could not be clearly observed in the $Al_{88-X}Si_{12}Mn_X$ ($X = 1$, 5, and 7) anodes, which may be likely that the lithiation reaction did not occur in the given voltage range. For the $Al_{83}Si_{12}Mn_5$ and $Al_{81}Si_{12}Mn_7$ anodes, the current peaks became very broad, indicating that Li was the solute atom stored in the anode and formed solid solution. When the Mn content was 13 %, the cathodic current peak was sharp, and a cathodic current peak appeared at near 0.15 V. According to the XRD results shown in Fig. 5 and Refs. [5, 10], it could be concluded that the cathodic current peaks appeared at near 0.15 V due to the formation of AlLi, while the anodic peaks appeared at 0.65 V because of its decomposition. More obvious cathodic peak and sharper anodic peak appeared in $Al_{75}Si_{12}Mn_{13}$, indicating that a great quantity of AlLi intermetallic compound was formed. Besides, the evidence of lithiation of α-Si did not occur in the present investigation.

The morphology of the melt-spun $Al_{88-X}Si_{12}Mn_X$ anodes after several cycles is presented in Fig. 7. Serious cracks of powders (Fig. 7a) could be observed in $Al_{85}Si_{12}Mn_3$, and slight cracks appeared on the surface of the $Al_{83}Si_{12}Mn_5$ and $Al_{81}Si_{12}Mn_7$ anodes after 50 cycles (Fig. 7b, c). The more serious cracks could be observed in $Al_{78}Si_{12}Mn_{10}$ after cycles (Fig. 7d). For the $Al_{75}Si_{12}Mn_{13}$ anode, the obvious pulverization of the particles appeared after cycles (Fig. 7e). The pulverization and cracks responded to capacity fade in the present investigation.

4 Discussion

The experiments revealed that when the Mn content was 1 %, the as-quenched ribbons were composed of supersaturated solid solution α-Al with large sizes, and α-Si spread along the α-Al grain boundaries, and performed

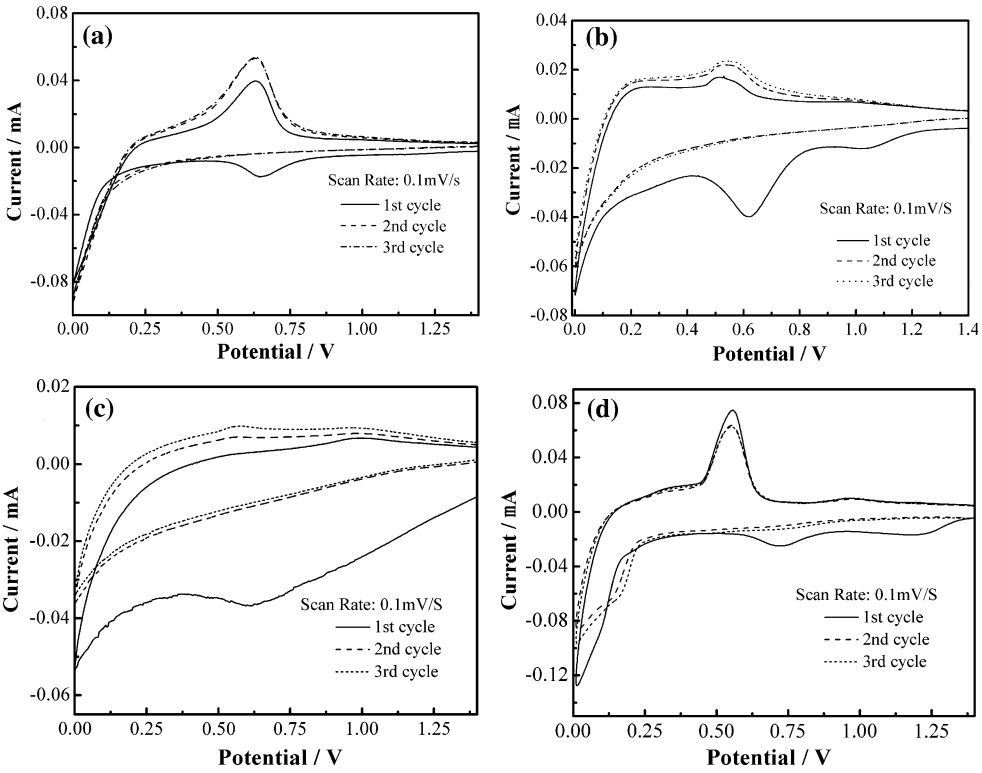

Fig. 6 Cyclic voltammetric curves for the as-quenched $Al_{87}Si_{12}Mn_1$ (**a**), $Al_{83}Si_{12}Mn_5$ (**b**), $Al_{81}Si_{12}Mn_7$ (**c**) and $Al_{75}Si_{12}Mn_{13}$ (**d**) anodes

high initial capacities but fast capacity fade. As the Mn content was increased to 5–7 %, the alloys were constituted of the nanoscaled α-Al and amorphous regions and their capacities reduced, but cycle performances were improved effectively. When the Mn content was more than 10 %, the alloys which were constituted of the intermetallic compound $Al_{4.01}MnSi_{0.74}$ and large scaled α-Al presented a much higher initial capacity, but fast capacity fade. The results reveal that the phase constitution and microstructure have a key influence on electrochemical properties.

In our prior work [15, 16], it was considered that two or three phases could co-exist in the solid solution during lithiation. A solid solution of Li in α-Al will form as Li is inserted into the melt-spun Al–Si–Mn supersaturated solid solution anodes with large solubility of Li. In the present work, the supersaturated Al-based solid solution and amorphous regions with three components co-existing in the ribbons and the intermetallic compounds with Li were not detected in the lithiated alloys when the Mn content was less than 7 %. These results confirm that Li is mainly stored in the supersaturated α-Al. The lithiation reaction of α-Al in the present work is similar to that of the melt-spun Al–Si–Mn alloys with high Si content. The α-Al grains in the melt-spun $Al_{83}Si_{12}Mn_5$ and $Al_{81}Si_{12}Mn_7$ ribbons were nanoscaled and surrounded by amorphous regions. No evidence revealed that the metallic glass crystallized during cycles, and the prior work presented that the metallic glass exhibited some capacities and excellent cycle performance [19]. According to the additional Ref. [20], the atom arrangement of the metallic glass is usually loose and the activation energy is lower compared with that of crystals, leading to the relatively high diffusion coefficient. Meanwhile, nanoscaled grains result in lots of grain boundaries with the rapid diffusion media. Consequently, the microstructure that nanoscaled grains co-existed with the amorphous regions could improve the atoms diffusion ability. Furthermore, the volume expansion of α-Al caused by the insertion of Li atoms could be restrained by the metallic glass. This effect is very helpful to improve the cycle performance. As the metallic glass was limited, the function was in shortage, resulting in excess expansion and poorer cycle performance when the Mn content was 1 and 3 %. It is more important that the melt-spun $Al_{88-X}Si_{12}Mn_X$ had high plasticity and high toughness because only little α-Si or Al/Si/Mn compounds appeared when X was in a range of 1–7 %. The high plasticity and toughness could mitigate the appearance of cracks during cycles, which is very beneficial to obtaining a more stable cycle performance. According to the classical material science theory (the Thompson-Freudlich Formula), the smaller the grain size, the larger the solubility obtained. In addition, nanoscaled grain size caused the huge increase of grain boundaries, which would increase the solubility of Li in α-Al and the metallic glass too. So, an improved performance was exhibited in $Al_{83}Si_{12}Mn_5$ and $Al_{81}Si_{12}Mn_7$.

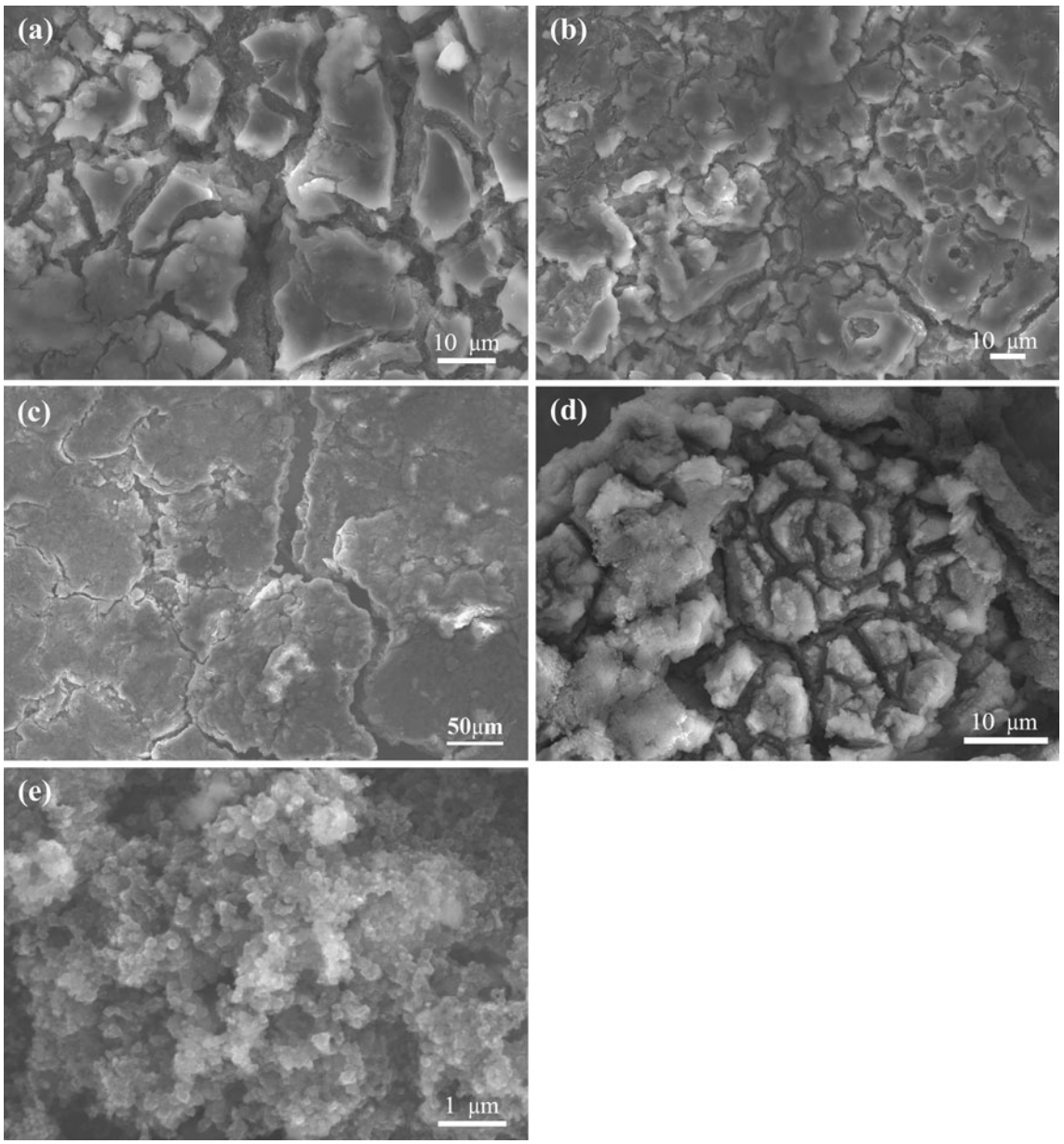

Fig. 7 Morphology of the lithiated $Al_{85}Si_{12}Mn_3$ (**a**), $Al_{83}Si_{12}Mn_5$ (**b**), $Al_{78}Si_{12}Mn_{10}$ (**c**) and $Al_{75}Si_{12}Mn_{13}$ (**d**) anodes after cycles

However, for the $Al_{75}Si_{12}Mn_{13}$ alloy, the intermetallic compound $Al_{4.01}MnSi_{0.74}$ existed as the prime phase and a high initial capacity of 1,176 mAh g^{-1} presented (Figs. 2, 4). The results indicated that the compound appeared in the $Al_{88-X}Si_{12}Mn_X$ could be alloyed by Li. A plenty of AlLi compounds could be measured after lithiation (Figs. 5, 6), which meant that the compound to be decomposed was accompanied by a serious pulverization (Fig. 7e). Meantime, the plasticity and toughness were also inferior because of the coarsening of grains and disappearance of amorphous regions. A conclusion can be drawn that the type of intermetallic compounds has an important influence on lithiation mechanism.

5 Summary

When $X = 1$ and 3, the as-quenched $Al_{88-X}Si_{12}Mn_X$ alloys were composed of coarse supersaturated solid solution α-Al grains, and α-Si spread along the boundaries and performed high initial capacities but fast capacity fade. As $X = 5$ and 7, the alloys were constituted by the nanoscaled α-Al and amorphous regions, and they exhibited capacities of 924 and 764 mAh g^{-1} initially and then maintained reversible capacities of 391 and 351 mAh g^{-1} after 50 cycles, respectively. When the Mn content was more than 10 %, an intermetallic compound $Al_{4.01}MnSi_{0.74}$ evolved into the predominated constitution. The initial specific capacities

were very high, but faded rapidly only experiencing few cycles. After lithiation, any compounds with Li could not be detected in the $Al_{85}Si_{12}Mn_3$ and $Al_{83}Si_{12}Mn_5$ anodes, while the AlLi intermetallic compound could be observed when the Mn content was increased to 13 %. It could be considered that the appropriate phase constitution of the $Al_{83}Si_{12}Mn_5$ and $Al_{81}Si_{12}Mn_7$ anode can effectively restrain the structure evolution, improve the structure stability, and obtain favorable electrochemical properties. The $Al_{4.01}MnSi_{0.74}$ compound was an active phase for Li storage in the present system but it was responsible for serious structure evolution, pulverization and poor cyclability.

Acknowledgments This work was supported by the National Natural Science Foundation of China (50871081, 51002117, 51071117).

References

1. Fan XY, Zhuang QC, Wei GZ, Huang L, Dong QF, Sun SG (2009) J Appl Electrochem 39:1323–1330
2. Chen LB, Xie JY, Yu HC, Wang TH (2009) J Appl Electrochem 39:1157–1162
3. Liu WR, Yen YC, Wu HC, Winter M, Wu NL (2009) J Appl Electrochem 39:1643–1649
4. Xiang JY, Wang XL, Zhong J, Zhang D, Tu JP (2011) J Power Sources 196:379–385
5. Hu RZ, Zeng MQ, Li CYV, Zhu M (2009) J Power Sources 188:268–273
6. Mirzadeh H, Zomorodian A (2010) Mater Sci Technol 26:281–284
7. Huang L, Cai JS (2009) Electrochem Commun 11:950–953
8. Padmavathy P, Ananthakumar R, Subramanian B, Ravidhas C, Jayachandran M (2011) J Appl Electrochem 41:751–756
9. Lee YS, Lee JH (2006) Electrochim Acta 52:1523–1526
10. Chen ZX, Qian JF, Ai XP, Cao YL, Yang HX (2009) Electrochim Acta 54:4118–4122
11. Huang KL, Zhang G, Liu SQ (2007) Trans Nonferr Metal Soc China 17:841–845
12. Park CM, Sohn HJ (2010) J Electrochem Soc 157:A46–A49
13. Park SE, Kim BE, Lee SW, Lee JK (2009) Trans Nonferr Metal Soc China 19:1023–1026
14. Hauser JJ, Chen HS, Espinosa GP, Waszczak JV (1986) Phys Rev B 34:674–4678
15. Sun ZB, Wang XD, Li XP, Zhao MS, Li Y, Zhu YM, Song XP (2008) J Power Sources 182:353–358
16. Sun ZB, Li XP, Wang XD, Hu Q, Zhao MS, Zhu YM, Li Y, Song XP (2009) Sci China Ser E 52:2288–2294
17. Suresh P, Shukla AK, Shivashankar SA, Munichandraiah N (2002) J Power Sources 110:11–18
18. Lee SE, Kim EJ, Cho J (2007) Electrochem Solid-State Lett 10:A1–A4
19. Zhang LP, Song XP, Wang F, Hu Q, Sun ZB, et al. (2012) J Solid State Electrochem 16:2159–2167
20. Kittel C (2005) Introduction to solid state physics. Wiley, New York